University of Dundee

A comparative study of turbulence models in a transient channel flow

Gorji, S.; Seddighi, M.; Ariyaratne, C.; Vardy, Alan; O'Donoghue, T.; Pokrajac, D.; He, S.

[Link to publication in Discovery Research Portal](#)

CrossMark

A comparative study of turbulence models in a transient channel flow

S. Gorji [a], M. Seddighi [a], C. Ariyaratne [b], A.E. Vardy [c], T. O'Donoghue [d], D. Pokrajac [d], S. He [a,*]

[a] Department of Mechanical Engineering, University of Sheffield, Sheffield S1 3JD, UK
[b] Thermo-Fluid Mechanics Research Centre, University of Sussex, Brighton BN1 9QT, UK
[c] Division of Civil Engineering, University of Dundee, Dundee DD1 4HN, UK
[d] School of Engineering, University of Aberdeen, Aberdeen AB24 3UE, UK

ABSTRACT

The performance of a number of low-Reynolds number turbulence models is evaluated against direct numerical simulations (DNS). All models are applied to an unsteady flow comprising a ramp-type excursion of flow rate inside a closed channel. The flow rate is increased linearly with time from an initial Reynolds number of 9308 (based on hydraulic diameter and bulk velocity) to a final Reynolds number of 29,650. The acceleration rate is varied to cover low, intermediate and high accelerations. It is shown that among the models investigated, the k–ε models of Launder and Sharma (1974) and Chang et al. (1995) [28] and the γ–Re_θ transition model of Langtry and Menter (2009) [38] capture well the key flow features of these unsteady turbulent flows. For the cases of low and intermediate acceleration rates, these three models yield predictions of wall shear stress that agree well with the corresponding DNS data. For the case of high acceleration, the γ–Re_θ model of Langtry and Menter (2009) [38] and the k–ε model of Launder and Sharma (1974) yield reasonable predictions of wall shear stress.

© 2013 Elsevier Ltd. All rights reserved.

1. Introduction

Unsteady turbulent flows are of interest to turbulence researchers because of their wide range of occurrence across many engineering disciplines. A large amount of on-going research is leading to a better understanding of the complex turbulence mechanisms present in such flows. Studies of unsteady turbulent flows are mainly conducted through two main categories; periodic and non-periodic.

Numerical and experimental techniques have been employed to investigate the turbulent flow features associated with periodic changes of flow rate with time. Brereton and Mankbadi [1] and Gündoğdu and Çarpinlioğlu [2] present comprehensive reviews. The experimental studies of Gerrard [3], Mizushina et al. [4], Shemer et al. [5], Mao and Hanratty [6], Tardu et al. [7] and He and Jackson [8] and the numerical studies of Scotti and Piomelli [9,10] and Cotton et al. [11] are all examples of such research. The research includes study of the flow behaviour for a range of frequency, amplitude and mean flow rates in the case of pulsating flow. Efforts on correlating the data on such flows have led to non-dimensional parameters representing the extent to which shear waves generated attenuate in terms of wall units.

The experimental studies of Maruyama et al. [12], Lefebvre [13], He and Jackson [14], Greenblatt and Moss [15,16] and He et al. [17] are examples of research on non-periodic flows, while the numerical investigations of Chung [18], He et al. [19], Ariyaratne et al. [20], Seddighi et al. [21], Di Liberto and Ciofalo [22], Jung and Chung [23] and He and Seddighi [24] examined the effects of sudden changes in pressure gradient or of linear ramp up/down in flow rates.

He and Jackson [14] focused their research on linearly increasing and decreasing flow rate in fully developed pipe flows. They identified three delays associated with the response of turbulence. Delays in turbulence production, turbulence energy redistribution and turbulence radial propagation were found to be the key features of such unsteady turbulent flows. It was found that the first response of turbulence to the imposed flow rate initiates from a region close to the wall where turbulence production is highest (buffer layer). The axial component of the Reynolds stress is the first to respond to the excursion while the other two normal components experience a longer delay. Eventually response of turbulence to the excursion is propagated towards the pipe centre due to the action of turbulent diffusion.

He et al. [19] identified three stages in the development of wall shear stress in ramp-type flow rate excursions through numerical studies. The first stage corresponds to the period of delay in turbulence response (frozen turbulence), occurring when inertial forces are dominant. This stage covers the period when wall shear stress first overshoots and then undershoots the corresponding quasi-steady values. He et al. [19] showed that a non-dimensional parameter involving inner turbulence time scales associated with the turbulence production correlates very well with the unsteady wall shear stress. It was shown by He and Ariyaratne [25] that

during this first stage the unsteady component of the wall shear stress behaves in a laminar-like manner. The second stage begins with the generation of new turbulence which causes the wall shear stress to escalate. It is shown by He et al. [17] that a correlation exists between the outer turbulence time scales and the critical Reynolds number at which transition from stage one to two occurs. The third stage includes the period when the wall shear stress asymptotically approaches the corresponding quasi steady trend. He et al. [19] also investigated the effects of fluid properties on the unsteady wall shear stress behaviour. For this purpose, two flow cases with different working fluids (water and air) but identical Reynolds range and acceleration rate were examined. It was shown that the unsteady wall shear stress deviation from the corresponding quasi-steady values is much smaller for air than for water because of water's higher density.

The ability of Reynolds Averaged Navier–Stokes (RANS) models to predict the flow behaviour of steady/unsteady channel/pipe flows has been investigated by a number of researchers. The studies of Patel et al. [26], Myong and Kasagi [27] and Chang et al. [28] are some good examples of application of RANS models to steady pipe/channel flows. Sarkar and So [29] investigated the performance of different turbulence models for steady channel flows (along with Couette, boundary layer and back-step flows). They examined ten different low-Reynolds number turbulence models, comparing their results with available DNS and experimental data. They observed that models with asymptotically consistent near wall behaviour generally return better predictions of flow features. Asymptotic behaviour of the turbulent kinetic energy, its dissipation rate and the Reynolds shear stress near a wall is explained by Launder [30].

Performance of RANS models in unsteady flows have been studied by Cotton et al. [11], Scotti and Piomelli [10], Tardu and Da Costa [31], Al-Sharif et al. [32], Khaleghi et al. [33] and Revell et al. [34]. The performance of turbulence models in predicting features of unsteady flows differ according to the turbulence model formulations. In most cases researchers compare the performance of different models against the available experimental or DNS data. Cotton et al. [11] examined the performance of the second-moment closure model of Shima [35] and the $k–\varepsilon$ model of Launder and Sharma [36] for both oscillatory flat-plate boundary layer and pulsatile pipe flow. It was found that the second-moment closure schemes generally performed better in comparison with the $k–\varepsilon$ model examined. Scotti and Piomelli [10] assessed the performance of five turbulence models against their own DNS data on pulsating flows (Scotti and Piomelli [9]), while Khaleghi et al. [33] investigated the performance of four turbulence models for a ramp-up pipe flow, comparing their results with the experimental data of He and Jackson [14]. In each of these two studies, the performance of an algebraic one-equation model, a $k–\varepsilon$ model, a $k–\omega$ model and a $k–\varepsilon–v^2$ model were examined. It was concluded from both studies that $k–\varepsilon–v^2$ model outperforms the rest. However, these conclusions were based on investigations of only a limited number of models among the various formulations. Furthermore, new turbulence models have recently been developed which were not considered by previous researchers.

The present paper reports on a systematic study of the performance of a wide range of low-Reynolds number turbulence models used to predict the detailed flow characteristics of ramp-up-type unsteady flows in a channel. Recent DNS results are used as benchmark data for the assessment.

2. Methodology

The study reported here involves the assessment of ten different turbulence models applied to three accelerating flow test cases.

FLUENT 13.0 is used as the RANS solver for the numerical investigations.

The flow domain consists of a rectangular channel section with smooth wall boundaries and the working fluid is water ($\rho = 1000$ kg/m^3, $v = 1 \times 10^{-6}$ m^2/s). The channel is 8 m long and 0.05 m high, giving a length to height ratio of $L/H = 160$ as shown in Fig. 1. Because of symmetry, the computational domain covers half the channel height. In this study, only spatial fully developed flow is of interest; hence, the results presented are taken at 7.5 m from the inlet ($L/H = 150$, AB line in Fig. 1). Systematic mesh sensitivity tests were carried out for each group of turbulence models to obtain mesh-independent solutions. These tests were conducted by distributing 70, 100 and 180 control volumes in the wall normal direction (y direction, shown in Fig. 1). It was concluded that distributing 100 control volumes non-uniformly along the wall normal direction is adequate to achieve mesh independent solutions. The number of control volumes used in the axial direction (x direction, shown in Fig. 1) is 30 but this is of no significance since only axially developed flow is of interest. This also means that the level of turbulence intensity at the inlet is of no relevance as long as it is set to a sufficiently high level to initiate turbulence in the pipe. In this work, it is set to be 5% in all simulations. The non-dimensional distance of the first node from the wall is maintained within the range of $y^+ = 0.3$–0.9 ($y^+ = yu_\tau/v$, u_τ representing friction velocity) during the excursion to ensure the low-Reynolds criterion for the models is satisfied.

In all test cases the flow rate is increased linearly from an initial steady state Reynolds number ($Re_0 = U_{b0}D_h/v$, U_{b0} representing the bulk velocity) of 9308 to a final Reynolds number (Re_1) of 29,650. The length scale of the Reynolds number is based on the hydraulic diameter, i.e. $D_h = 2H$, where H is the full height of the channel. We consider three acceleration time periods (T): Case A, 8.16 s ("low" acceleration); Case B, 2.86 s ("intermediate" acceleration); Case C, 0.02 s ("high" acceleration). Table 1 summarises the initial and final flow conditions of examined flow cases along with non-dimensional time scale $\Delta t^* = T/(H/2)/U_{b1}$ and ramp rate ($dU/dt = (U_{b1}-U_{b0})/T$). Although these simulations are carried out for water, as long as the boundary conditions such as the initial and final Reynolds numbers and non-dimensional acceleration rate are consistent, the choice of fluid is of no significance to the outcome of the simulations.

The continuity and momentum transport equations along with the Reynolds stress closure equations are solved for the computational domain. The flow is assumed to be two-dimensional and Cartesian coordinates are employed for the governing equations.

Continuity:

$$\frac{\partial U_i}{\partial x_i} = 0 \tag{1}$$

Momentum:

$$\frac{DU_i}{Dt} = -\frac{1}{\rho}\frac{\partial P}{\partial x_i} + \frac{\partial}{\partial x_i}\left(v\frac{\partial U_i}{\partial x_j} - \overline{u_i u_j}\right) \tag{2}$$

where linear eddy viscosity models employ a stress–strain relation as follows:

$$\overline{u_i u_j} = 2/3k\delta_{ij} - v_t\left(\frac{\partial U_i}{\partial x_j} + \frac{\partial U_j}{\partial x_i}\right) \tag{3}$$

where v_t, the eddy viscosity, is obtained by solving a set of turbulence transport equations, the details of which are presented in the next sections.

Only low-Reynolds number turbulence models can potentially predict the features of unsteady flows. Here we consider ten low-Reynolds turbulence models, which can be categorised into four
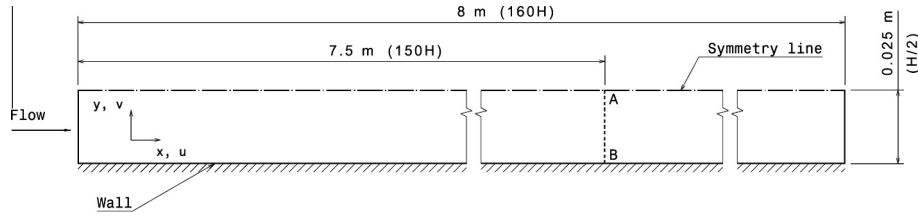
Fig. 1. Sketch of the channel geometry.

Table 1
Test cases and flow conditions.

Flow case	Re_0	Re_1	Δt^*	T (s)	dU/dt (m/s^2)
A	9308	29,650	96.8	8.16	0.025
B	9308	29,650	33.9	2.86	0.071
C	9308	29,650	0.2	0.02	10.17

Note: $\Delta t^* = \frac{T}{(H/2)/U_{b1}}$; $\frac{dU}{dt} = \frac{U_{b1}-U_{b0}}{T}$.

Table 2
Constants for the turbulence models.

Model	C_μ	$C_{\varepsilon1}$	$C_{\varepsilon2}$	σ_k	σ_ε
AB	0.09	1.45	1.83	1.0	1.4
LB	0.09	1.44	1.92	1.0	1.3
LS	0.09	1.44	1.92	1.0	1.3
YS	0.09	1.44	1.92	1.0	1.3
AKN	0.09	1.5	1.90	1.4	1.4
CHC	0.09	1.44	1.92	1.0	1.3

groups: k–ε models, k–ε based models, the v^2–f model of Durbin [37] and the γ–Re_θ transition model of Langtry and Menter [38].

2.1. k–ε models

Low-Reynolds number k–ε turbulence models are based on solving transport equations for turbulent kinetic energy and its dissipation rate, as follow:

$$\frac{Dk}{Dt} = \frac{\partial}{\partial x_j}\left[\left(v + \frac{v_t}{\sigma_k}\right)\frac{\partial k}{\partial x_j}\right] + P_k - \tilde{\varepsilon} - D \tag{4}$$

$$\frac{D\tilde{\varepsilon}}{Dt} = \frac{\partial}{\partial x_j}\left[\left(v + \frac{v_t}{\sigma_\varepsilon}\right)\frac{\partial \tilde{\varepsilon}}{\partial x_j}\right] + C_{\varepsilon1}f_1\frac{1}{T_t}P_k - C_{\varepsilon2}f_2\frac{\tilde{\varepsilon}}{T_t} + E \tag{5}$$

where P_k is the production of turbulent kinetic energy given by

$$P_k = -\overline{u_i u_j}\frac{\partial U_i}{\partial x_j} \tag{6}$$

Eddy viscosity in k–ε models is defined to be $v_t = C_\mu f_\mu k^2/\varepsilon$, C_μ being a constant and f_μ being the damping function. T_t in Eq. (5) is a turbulent time scale, $\tilde{\varepsilon}$ is the modified isotropic dissipation rate, D and E are near wall correction functions for k and ε equations, respectively.

The six k–ε turbulence models examined in this study are designated as AB for Abid [39], LB for Lam and Bremhorst [40], LS for Launder and Sharma [36], YS for Yang and Shih [41], AKN for Abe et al. [42] and CHC for Chang et al. [28]. Note that the performance of FLUENT's built-in LS model is found to be unexpectedly poor and therefore a User Defined Function (UDF) for LS developed by Mathur and He [43] was also implemented. The FLUENT built-in implementation of LS is designated LS-FLUENT and the UDF implementations is designated LS-UDF in what follows.

A summary of the model constants, damping functions and near wall correction functions are presented in Tables 2–4.

2.2. k–ω and shear stress transport (SST) k–ω models

FLUENT 13.0 employs the low-Reynolds number k–ω model of Wilcox [44], which solves two transport equations, one for turbulent kinetic energy (same as for the k–ε models) and one for its specific dissipation rate ($\omega \propto \varepsilon/k$). Further details of this model can be found in Wilcox [44].

The k–ω Shear Stress Transport (SST) model developed by Menter [45] employs a blending function, which retains the near-wall

ω equation while switching to ε equivalent further from the wall. Further details of the model can be found in Menter [45].

2.3. v^2–f model

Anisotropy of the turbulence stresses is not addressed in linear eddy viscosity turbulence models. Durbin [46] replaced the *ad hoc* damping functions of the k–ε models by introducing the wall-normal stress $\overline{vv}$ as the velocity scale in the eddy viscosity formulation. An elliptic relaxation function is also solved to model the redistribution process of wall normal stress transport equation. However, due to difficulties of implementation of the original formulation, major commercial codes tend to use more numerically stable formulations. The v^2–f version coded in FLUENT, which is examined in this study, is the due to Iaccarino [47] but with default constants of those proposed by Lien and Kalitzin [48].

2.4. γ–Re_θ transition model of Langtry and Menter [38]

The performance of a correlation based transition turbulence model of γ–Re_θ Langtry and Menter [38] available in FLUENT 13.0 is also considered. The model incorporates two extra transport equations into the SST model, one for the intermittency γ and the other for the transition onset momentum-thickness Reynolds number $\widetilde{Re}_{\theta t}$. Turbulent kinetic energy and its specific dissipation rate transport equations of the SST model are customised to include the additional transport equations.

The following are the transport equations for intermittency and momentum-thickness Reynolds number:

$$\frac{\partial\rho\gamma}{\partial t} + \frac{\partial\rho U_j\gamma}{\partial x_j} = P_\gamma - E_\gamma + \frac{\partial}{\partial x_j}\left[\left(\mu + \frac{\mu_t}{\sigma_f}\right)\frac{\partial\gamma}{\partial x_j}\right] \tag{7}$$

$$\frac{\partial\rho\widetilde{Re}_{\theta t}}{\partial t} + \frac{\partial\rho U_j\widetilde{Re}_{\theta t}}{\partial x_j} = P_{\theta t} + \frac{\partial}{\partial x_j}\left[\sigma_{\theta t}(\mu + \mu_t)\frac{\partial\widetilde{Re}_{\theta t}}{\partial x_j}\right] \tag{8}$$

where P_γ and E_γ are production and dissipation terms of the intermittency transport equation, respectively. $P_{\theta t}$ is the production term of momentum-thickness in the Reynolds number transport equation. σ_f and $\sigma_{\theta t}$ are the constants of intermittency and momentum-thickness Reynolds number transport equations, respectively.

Intermittency is a measure of the regime of the flow. For instance, in a growing boundary layer over a flat plate, intermittency is zero before the transition onset and reaches a value of one when

Table 3
Functions in the turbulence models.

Model	f_μ	f_1	f_2
AB	$\tanh(0.008 Re_k) \times \left(1 + \frac{4}{Re_t^{3/4}}\right)$	1.0	$1 - 2/9 \exp\left(-\frac{Re_t^2}{36}\right) \times \left(1 - \exp\left(-\frac{Re_k}{12}\right)\right)$
LB	$(1 - \exp(-0.0165 Re_y))^2 \times (1 + \frac{20.5}{Re_t})$	1.0	$1 - \exp(-Re_t^2)$
LS	$\exp\left(\frac{-3.4}{(1+Re_t/50)^2}\right)$	1.0	$1 - 0.3 \exp(-Re_t^2)$
YS	$(1 + 1/\sqrt{Re_t}) \times \left[1 - \exp\begin{pmatrix} -1.5 \times 10^{-4} Re_y \\ -5.0 \times 10^{-7} Re_y^3 \\ -1.0 \times 10^{-10} Re_y^5 \end{pmatrix}\right]^{0.5}$	$\frac{\sqrt{Re_t}}{1+\sqrt{Re_t}}$	$\frac{\sqrt{Re_t}}{1+\sqrt{Re_t}}$
AKN	$[1 + \frac{5}{Re_t^{0.75}} \exp(-(\frac{Re_t}{200})^2)] \times \left(1 - \exp\left(-\frac{y^*}{14}\right)\right)^2$	1.0	$\left\{1 - 0.3 \exp\left(-\left(\frac{Re_t}{6.5}\right)^2\right)\right\} \times \left(1 - \exp\left(-\frac{y^*}{3.1}\right)\right)^2$
CHC	$[1 - \exp(-0.0215 Re_y)]^2 \times (1 + \frac{31.66}{Re_t^{5/4}})$	1.0	$[1 - 0.01 \exp(-Re_t^2)] \times [1 - \exp(-0.0631 Re_y)]$

Table 4
D and E terms along with the boundary conditions.

Model	D	E	Wall BC
AB	0	0	$\varepsilon_w = \nu\left(\frac{\partial^2 k}{\partial y^2}\right)$
LB	0	0	$\varepsilon_w = \nu\left(\frac{\partial^2 k}{\partial y^2}\right)$
LS	$2\nu\left(\frac{\partial \sqrt{k}}{\partial y}\right)^2$	$2\nu\nu_t\left(\frac{\partial^2 U}{\partial y^2}\right)^2$	$\tilde{\varepsilon}_w = 0$
YS	0	$\nu\nu_t\left(\frac{\partial^2 U}{\partial y^2}\right)^2$	$\varepsilon_w = \nu\left(\frac{\partial^2 k}{\partial y^2}\right)$
AKN	0	0	$\varepsilon_w = \nu\left(\frac{\partial \sqrt{k}}{\partial y}\right)^2$
CHC	0	0	$\varepsilon_w = \nu\left(\frac{\partial^2 k}{\partial y^2}\right)$

Note: $Re_t = \frac{k^2}{\nu\varepsilon}$ $Re_y = \frac{yk^{1/2}}{\nu}$ $y^* = \frac{yu_\varepsilon}{\nu}$ $u_\varepsilon = (\nu\varepsilon)^{0.25}$.

the flow is fully turbulent. In order to determine the condition of a developing boundary layer, correlations exist between the location of the transition onset and the free stream turbulence intensity, pressure gradient and transition momentum-thickness Reynolds number (Abu-Ghannam and Shaw [49] and Mayle [50]). Both algebraic and transport equations have been developed by researchers to determine the intermittency factor. Langtry and Menter [38] couples the transport equations for intermittency and transition onset momentum-thickness Reynolds number to Menter [45] SST model. The production term in the turbulent kinetic energy transport equation is modified to account for the changes in the intermittency of the flow.

The transition onset momentum-thickness Reynolds number is mainly responsible for capturing the nonlocal effects of turbulence intensity and pressure gradient outside the boundary layer. Further details regarding the formulation of the model and its performance in different test cases can be found in Langtry and Menter [38].

3. Comparisons for steady flow

DNS results for two steady flow scenarios, corresponding to the initial and final Reynolds numbers (Re_0 = 9308 and Re_1 = 29650) of the unsteady flow cases to be discussed in the next section, are used to assess the performance of the ten different low-Reynolds number turbulence models applied to two-dimensional, fully developed, steady channel flow.

Fig. 2 shows the predications of mean axial velocity, turbulent kinetic energy, turbulent shear stress and turbulent viscosity with the DNS results for the initial and final Reynolds number flows. Bulk velocity (U_b) which represents the ratio of flow rate to cross sectional area and kinematic viscosity (ν) are used to normalise the mean and turbulence quantities.

All turbulence models with the exception of LS-FLUENT give an acceptable prediction of the axial velocity profile across the channel. However, the performance of the various models is rather different for the predictions of turbulent kinetic energy, turbulent shear stress and turbulent viscosity.

Most models are successful in predicting the location of the peak of turbulent kinetic energy for both steady flow cases. The predictions of the turbulent kinetic energy of LB, v^2–f and k–ω are the closest to DNS in the wall region, whereas the kinetic energy predictions of AB, AKN, CHC, LS-UDF and γ–Re_θ match better the DNS data in the core region. The last three models significantly under-predict the peak of turbulent kinetic energy for both flows even though they show superior performance in predicting the unsteady flows (as discussed in Section 4). It is of interest to note that γ–Re_θ transition SST and the basic k–ω SST give rather different predictions of the turbulent kinetic energy even for these steady fully developed turbulent flows. This is due to the fact that the intermittency becomes active in the inner and buffer layers of the wall shear flow where the local Reynolds number is low.

The turbulent shear stress is well predicted by AKN, LB, YS and γ–Re_θ. This contrasts with AB, CHC, LS-UDF and v^2–f, which slightly under-predict, and LS-FLUENT, which significantly over-predicts the shear stress. The turbulent viscosity predictions of most of the k–ε models are quite good in the wall region, with AKN, LB, YS and k–ω being the closest to DNS. In the core region, however, all models except AKN and k–ω predict a monotonic increase of eddy viscosity that is contrary to the DNS data. The over-prediction of eddy viscosity in this region is a known shortfall of many k–ε models that results from the under-prediction of dissipation (Billard and Laurence [51]). Myong and Kasagi [27] argue that in most k–ε models the chosen value of σ_k is too low in comparison to σ_ε and they therefore suggest using higher $\sigma_k/\sigma_\varepsilon$ ratios. In the absence of turbulent energy production in the core region, this ratio balances the diffusion and dissipation terms in the turbulent kinetic energy and its dissipation rate transport equations. Among the k–ε models investigated, AKN utilises the highest $\sigma_k/\sigma_\varepsilon$ ratio improving its eddy viscosity predictions in the core region.

It should be noted that in the framework of eddy viscosity models the only connection between the turbulence model and the mean flow field is through the turbulent shear stress $\overline{uv}$, which is mostly dependent on the eddy viscosity. It can be seen that $\overline{uv}$ is well predicted by all models (excluding LS-FLUENT) for both the high and the low Reynolds number flows. This is true despite the turbulent viscosity being not well predicted in the core region by some models. In fact, the most important part of the flow is the wall region, where the turbulent viscosity is predicted fairly well by most of the models. In the core region, the role of turbulent viscosity is not of major importance to the performance of the models.

Results obtained for the higher Reynolds number flow are generally more reliable (i.e. agree better with the DNS results) than those for the lower Reynolds number flow. We note that
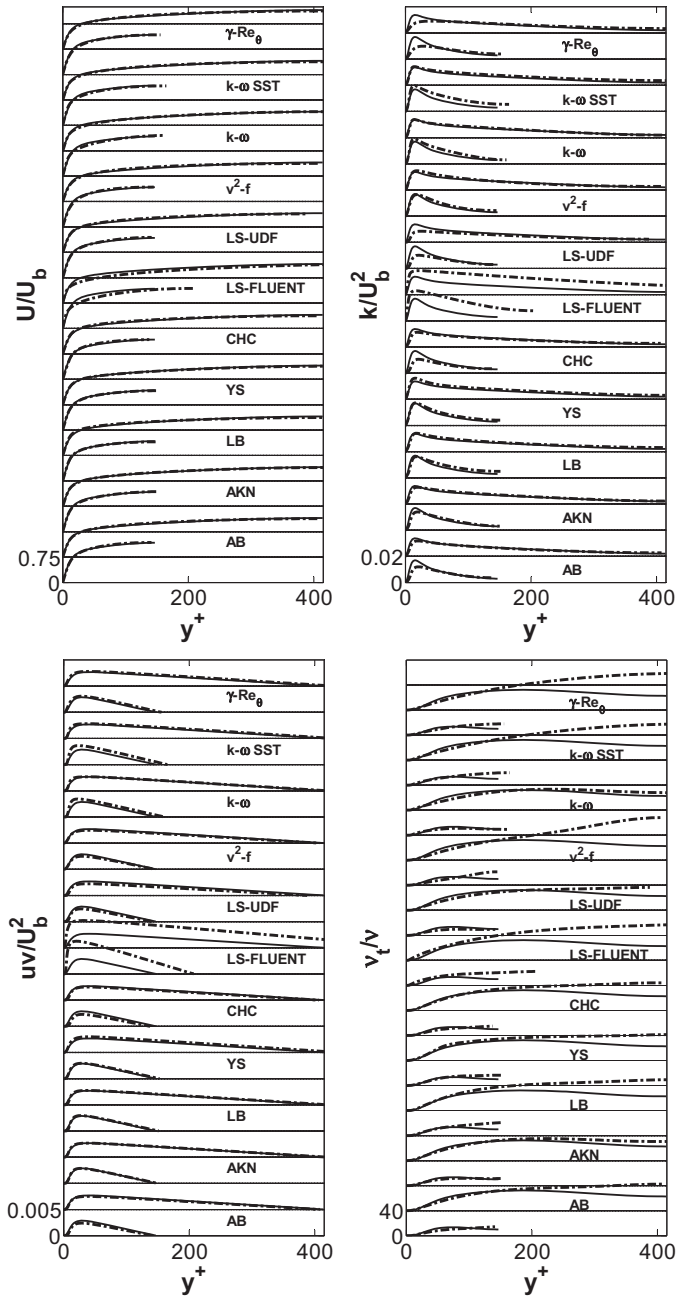
Fig. 2. Steady flows at $Re = 9308$ (short curves) and 29,650 (longer curves): Comparisons between predictions of various turbulence models (dashed line) with DNS data (solid line).

turbulence models are often tuned for relatively high Reynolds number flows, and applying such models to relatively low Reynolds number flows can result in poor performance.

Fig. 3 presents the wall shear stress predicted by the various turbulence models, together with the DNS results. Among the turbulence models considered, AKN, LB and $k–\omega$ are seen to yield the most accurate predictions of wall shear stress for both the lower and higher Reynolds number flows.

In contrast to the LS-FLUENT, LS-UDF performs well overall, leading to our conclusion that the poor performance of the FLUENT built-in LS model is due to its implementation within FLUENT, not due to any inherent fault with the model itself. The results obtained from LS-FLUENT are not further presented or discussed in the remainder of this paper.

4. Comparisons for unsteady flow

4.1. Key features of unsteady flow from DNS

The main features of the unsteady flows as predicted by DNS are first summarised in this section in order to facilitate the assessment of the performance of the turbulence models in the next section. The discussion largely follows that of He and Jackson [14], He et al. [17] and He and Seddighi [24], where more detailed discussion can be found.

Fig. 4 shows the DNS-predicted time histories of wall shear stress, turbulent viscosity, turbulent shear stress and turbulent kinetic energy for the three unsteady flow cases. Considering first the wall shear stress evolution for Case A (Fig. 4(a)), we can identify a three-stage development in the wall shear stress and turbulence. Stage 1 is initially dominated by large inertial effects, causing the wall shear stress to overshoot the corresponding quasi-steady values. However, due to the delayed turbulence response, the growth rate of wall shear stress decreases during the final moments of stage 1. Stage 2 corresponds to the time period when the generation of new turbulence causes the unsteady wall shear stresses to increase rapidly towards the corresponding quasi-steady values. During stage 3, the bulk flow is no longer accelerating and the wall shear stress gets gradually closer to the quasi-steady flow shear stress.

The flow acceleration is higher in Case B (Fig. 4(b)), and Re_1 is reached while flow response is still in stage 1 (a). As a result of the sudden removal of the acceleration, a strong but negative inertial effect is imposed on the flow, which results in a sharp decrease in the wall shear stress (stage 1 (b)). Afterwards, the trend is reversed when turbulence production starts to increase the wall shear stress, which eventually reaches the quasi-steady values. Increasing the acceleration even further (Case C, Fig. 4(c)) causes overshooting of the unsteady wall shear stress over the quasi-steady wall shear stress to occur in an instant (stage 1 (a), not shown on the figure), because of the very sudden change in flow rate. This is then followed by a sharp reduction (stage 1 (b)). During stage 2, the wall shear stress rapidly increases again as a result of turbulence production. The wall shear stress approaches the corresponding quasi steady values in stage 3.

The DNS-predicted time-histories of turbulent viscosity at selected y_0^+ locations (where $y_0^+ = y u_{\tau 0}/v$, $u_{\tau 0}$ representing friction velocity at Re_0) are also shown in Fig. 4. It can be seen from the Fig. 4 that turbulent viscosity close to the wall ($y_0^+ = 5$) remains more or less unchanged during stage 1, but begins to increase rapidly at approximately 5, 4 and 2 s for cases A, B and C respectively, corresponding to the onset of stage 2. It can also be seen that the delays of turbulent viscosity are roughly constant across the channel for all three flow cases. However, response of turbulent viscosity to the imposed excursion in the wall region is of greater importance for modelling purposes as discussed in Section 4.2.

The response of the turbulent shear stress is consistent with that of the turbulent viscosity. Turbulent shear stress very close to the wall (at $y_0^+ = 5$) stays mainly constant during stage 1. Its response to the acceleration is initially observed in the wall region, while the delay period becomes progressively longer with distance from the wall.

The overall picture of the development of turbulent kinetic energy with time is similar to that of turbulent shear stress. Delays associated with the response of turbulence increase with distance from the wall. However, the delay in turbulent kinetic energy in the wall region is much shorter than that for the shear stress. Also, turbulent kinetic energy increases slowly during stage 1, while turbulent shear stress and viscosity stay reasonably constant. During this period, the streamwise turbulent normal stress ($\overline{uu}$) increases
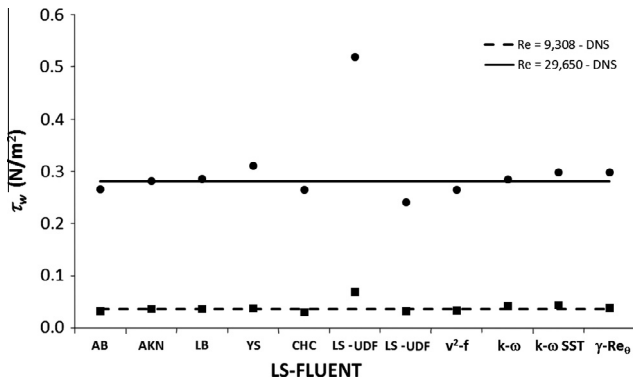
Fig. 3. Predictions of steady flow wall shear stress for two Reynolds numbers by the various turbulence models (symbols) and by DNS (lines).

due to the stretching of the existing eddies, while the turbulent shear stress ($\overline{uv}$), the wall-normal stress ($\overline{vv}$) and the spanwise stress ($\overline{ww}$) are unaffected (He and Jackson [14]). This strong anisotropic behaviour in the near-wall turbulence is the key feature of the unsteady flow and is likely to pose a challenge for linear eddy viscosity models.

4.2. Performance of the turbulence models

Fig. 5 shows the RANS models predictions of wall shear stress based on the various turbulence models for all three unsteady flow cases; the benchmark DNS results are also shown. It is seen that AB, CHC, LS, v^2–f and γ–Re_θ (referred to as Group I hereafter) capture the basic features of the flow exhibited by the DNS results rather well, whereas the other models (referred to as Group II) are not able to do so. All Group I models reproduce the three stage
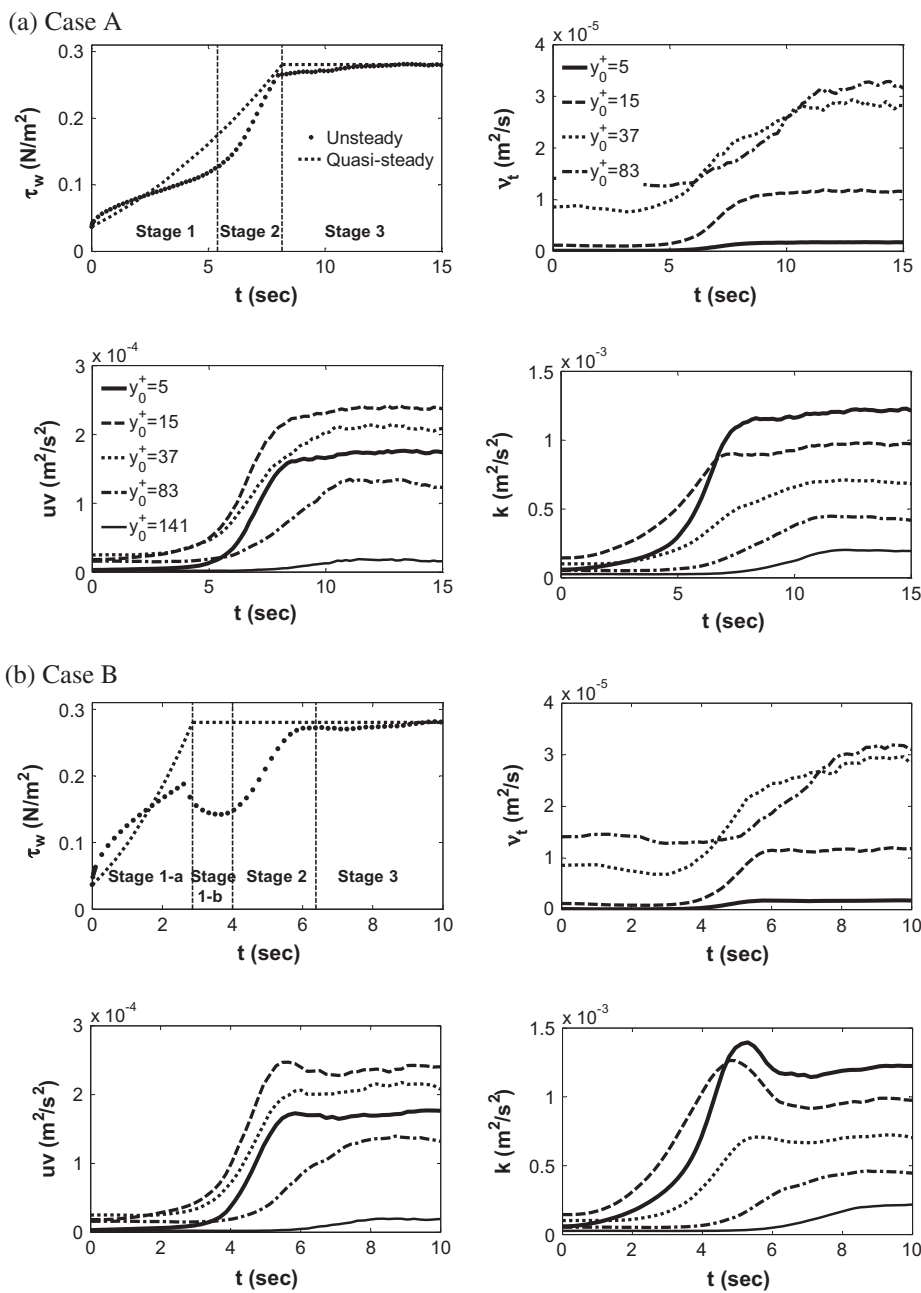

Fig. 4. Time-histories of wall shear stress and turbulence quantities in the three unsteady flow cases predicted by DNS.
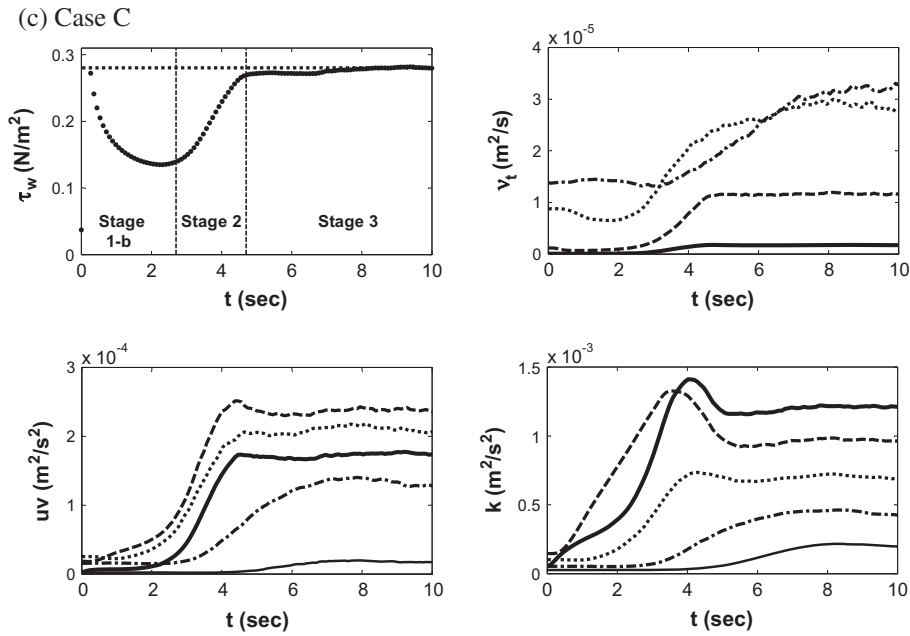
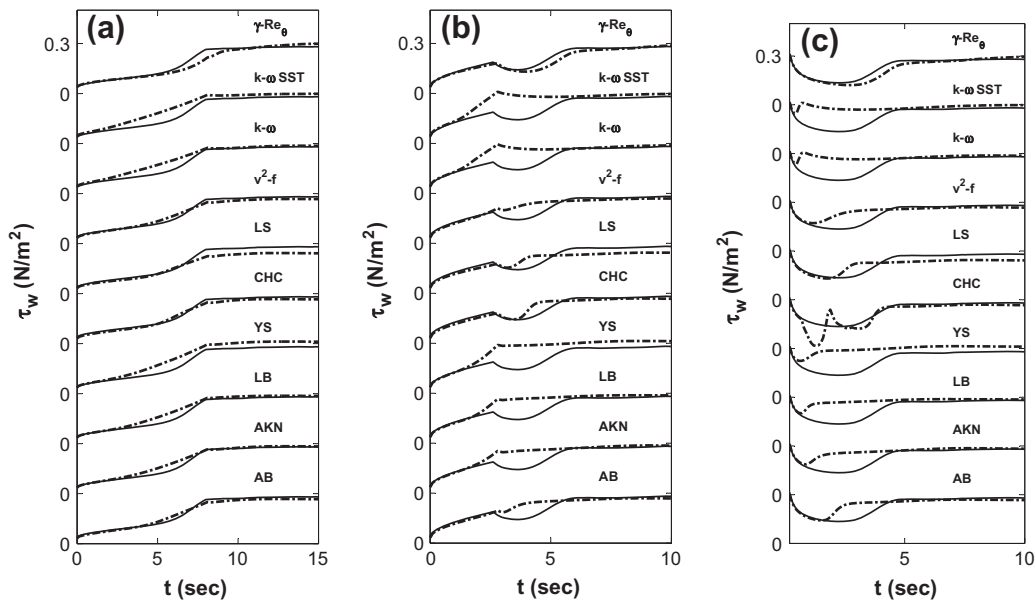(c) Case C

Fig. 4 (*continued*)

Fig. 5. Wall shear stress time-histories in unsteady flow cases; (a) Case A, (b) Case B and (c) Case C. DNS (solid lines) and RANS with various turbulence models (dashed lines).

development: a delay stage followed by a rapid response in stage 2 and then a slow adjustment phase (stage 3). Focusing on more detail, γ–Re_θ appears to predict time scales that are very close to those of DNS for all three flow cases. The LS and the CHC models predict time scales close to those of DNS, but are slightly shorter as the acceleration is increased. Note that CHC shows instability in the simulation of Case C. Although able to predict the general features of the unsteady turbulence response, the AB and v^2–f results always show time scales that are much shorter than those of DNS. The Group II models fail to predict the main features of the unsteady flows, mostly because of their inability to predict the delayed response of turbulence which controls the response of the flow. All of the models (both groups) are able to capture the initial overshoot of the shear stress in early stage 1 since this behaviour is due to the effect of the inertial forces, which is not strongly dependent on turbulence (and hence not dependent on

the choice of turbulence model). We note once more that the simulations of the LS model are based on the UDF version; predictions based on FLUENT's built-in LS model (not presented) are very different from the results described above, with very small delays that are much like the predictions of Group II models.

The model predictions of turbulent viscosity at $y_0^+ = 5$ due to the various models are shown in Fig. 6. The turbulent viscosity time histories reflect the trends in wall shear stress predicted by each model. It is apparent that the characteristic delay in turbulent viscosity in the wall region is well reproduced by LS, CHC and γ–Re_θ, and to some extent by AB and v^2–f. Once more, γ–Re_θ slightly over predicts the delays in all flow cases. CHC predicts the delay for flow Cases A and B rather accurately, whilst predicting unrealistic oscillation for flow Case C (not visible in the current scale of the figure). Even though v^2–f does not predict the delay period correctly for any of the cases, it is the only model to return accurate
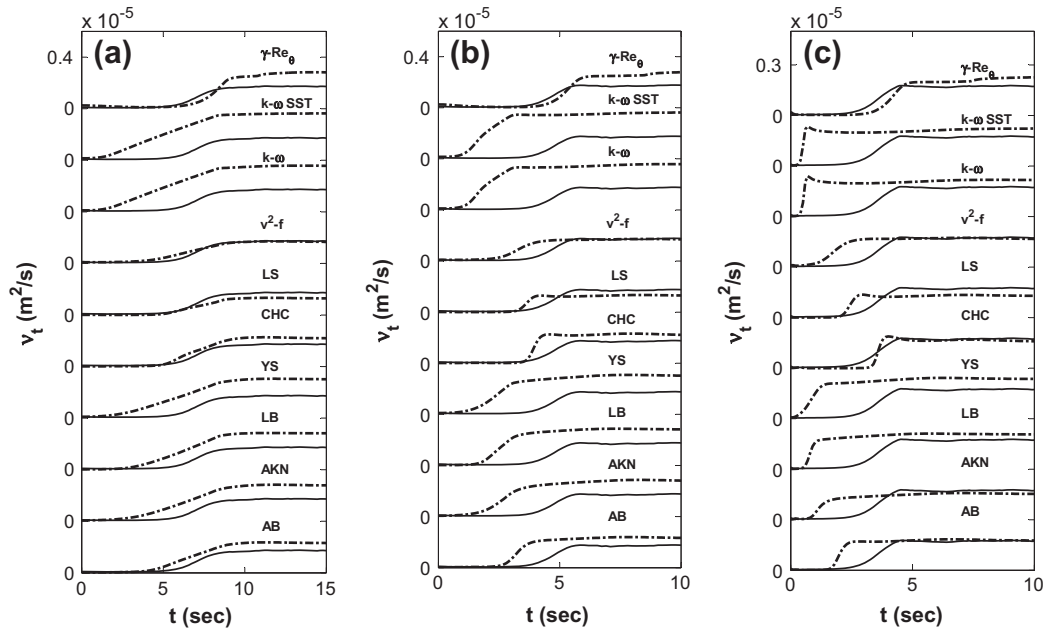
Fig. 6. Time-histories of turbulent viscosity at $y_0^+ = 5$ in unsteady flows; (a) Case A, (b) Case B and (c) Case C. DNS (solid lines) and RANS with various models (dashed lines).
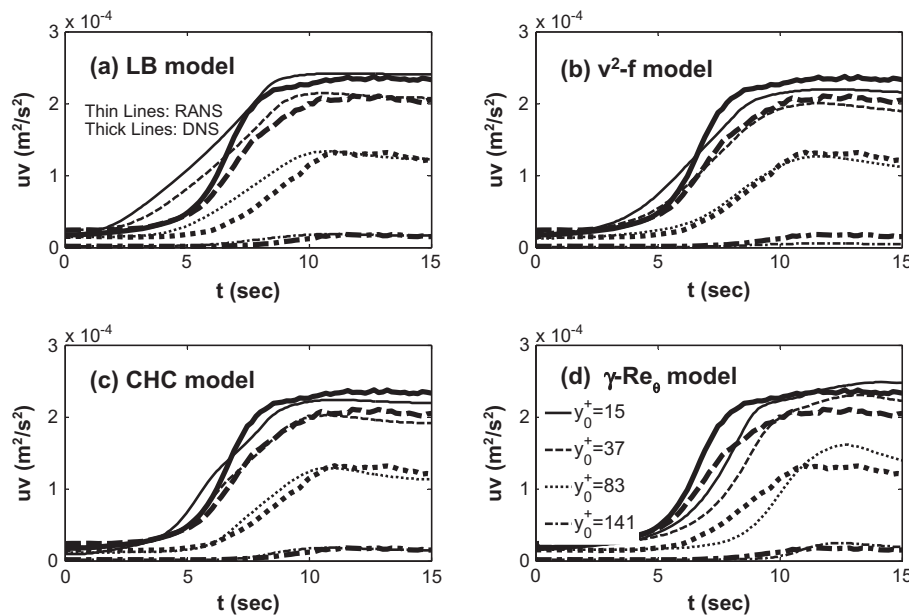

Fig. 7. Time-histories of turbulent shear stress at selected y_0^+ for unsteady flow case A: RANS model (thin lines) and DNS (thick lines).

values of turbulent viscosity during the pre- and post-ramp periods for all three flows. The delays predicted by AKN, LB and YS are much shorter than those of DNS, whereas k–ω and k–ω SST return even shorter delays. These observations are consistent with the predictions of wall shear stress from the respective models, as shown in Fig. 5.

Figs. 7–9 show the comparisons for turbulent shear stress. For brevity results obtained from selected turbulence models only are presented. Focusing on the wall region first ($y_0^+ = 15$), it is apparent that once more LS, CHC and γ–Re_θ (some not shown) predict the initial and the subsequent response rather well, whereas models AB, AKN, YS, LB and $\overline{v^2}$–f (some not shown) predict much shorter delays; hardly any delays are observed from the predictions of the k–ω and k–ω SST models (not shown). Considering the turbulent shear stress development in the core region, the

DNS data show progressively longer delays as one moves away from the wall. All models are capable of capturing this feature, with some models performing slightly better than others. The delay in the core region results from the fact that the turbulence response occurs initially in the wall region, propagating towards the centre through diffusion. The above comparison shows that all models are capable of reproducing this feature because the diffusion term is explicitly included in the transport equations of the turbulent kinetic energy and its dissipation rate. Once more CHC and γ–Re_θ are outperforming the rest in reproducing the trends associated with the development of turbulent shear stress across the channel; CHC's prediction for Case A is nearly indistinguishable from the DNS data although it is less so for Case B. In Case C, CHC's instability in predicting turbulence quantities in the wall region is once more evident in the trends of the turbulent shear stress. The LS
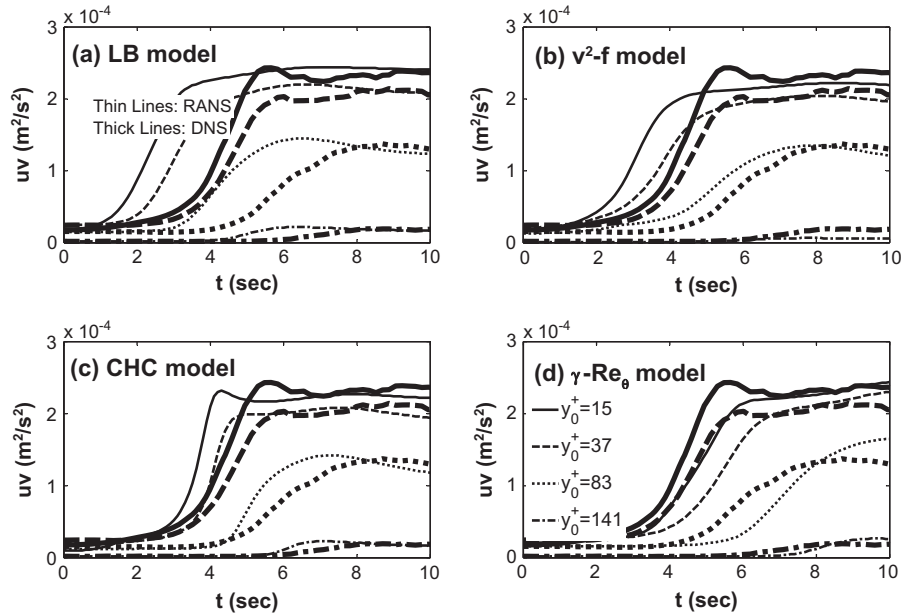
Fig. 8. Time-histories of turbulent shear stress at selected y_0^+ for unsteady flow case B: RANS model (thin lines) and DNS (thick lines).
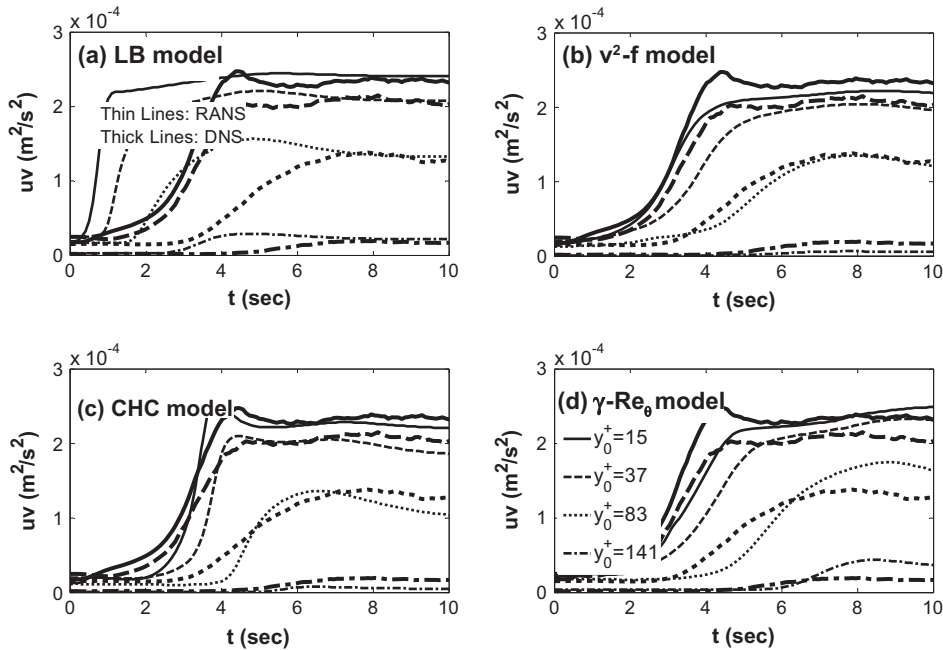

Fig. 9. Time-histories of turbulent shear stress at selected y_0^+ for unsteady flow case C: RANS model (thin lines) and DNS (thick lines).

model predicts the delay period fairly well, especially for cases A and B, but it returns magnitudes that are lower than those of DNS in the final plateau (not shown). The trends obtained by the AB and v^2–f are close to those of DNS only in the core region, failing to predict the delays close to the wall.

Figs. 10–12 show the predictions of turbulent kinetic energy for several wall-normal locations across the channel. Unlike turbulent shear stress, the turbulent kinetic energy shows a rather small delay in the wall region for the reasons explained in Section 4.1. It is interesting that all models except CHC, LS and γ–Re_θ can predict this near wall response fairly well. v^2–f prediction of turbulent kinetic energy in the wall region is almost indistinguishable from

the DNS data during the early stages of the three flows. γ–Re_θ on the other hand predicts a much longer delay, which is similar to that of the turbulent shear stress (it is noted that the important requirement for any eddy viscosity model is to faithfully represent the turbulent viscosity itself or the turbulent shear stress). In this particular case, since turbulent kinetic energy and shear stress show different characteristics, it is actually desirable that the early response of the kinetic energy is not reproduced so that the turbulent shear stress ($\overline{uv}$) can be well represented. This is what CHC, LS and γ–Re_θ have done in order to capture the delay of the wall shear stress correctly. Clearly it is desirable for a model to decouple the prediction of turbulent shear stress and the prediction of turbulent
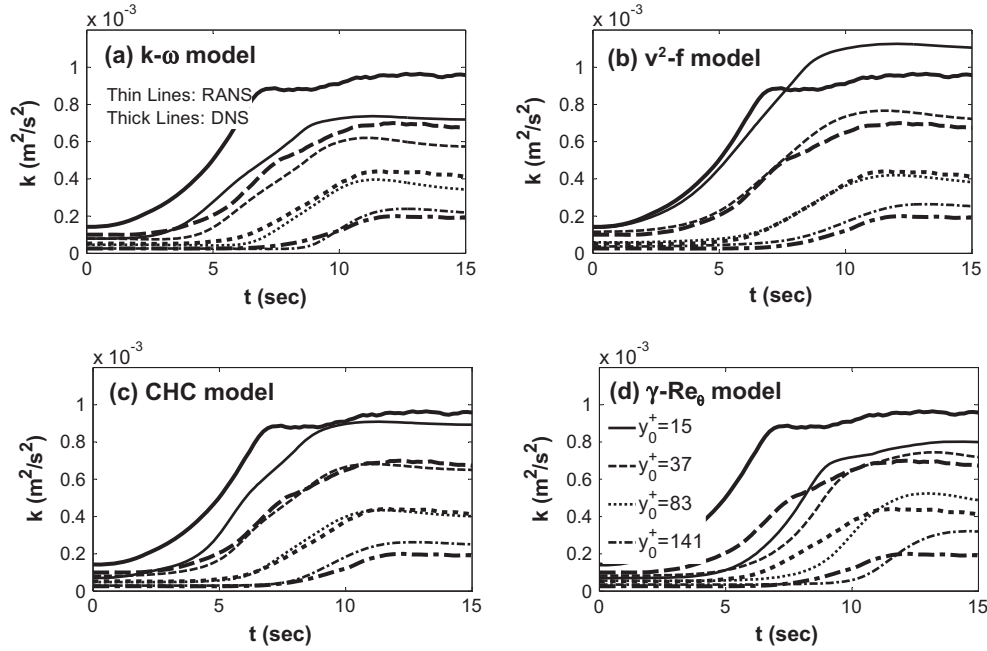
Fig. 10. Time-histories of turbulent kinetic energy at selected y_0^+ for unsteady flow case A: RANS model (thin lines) and DNS (thick lines).
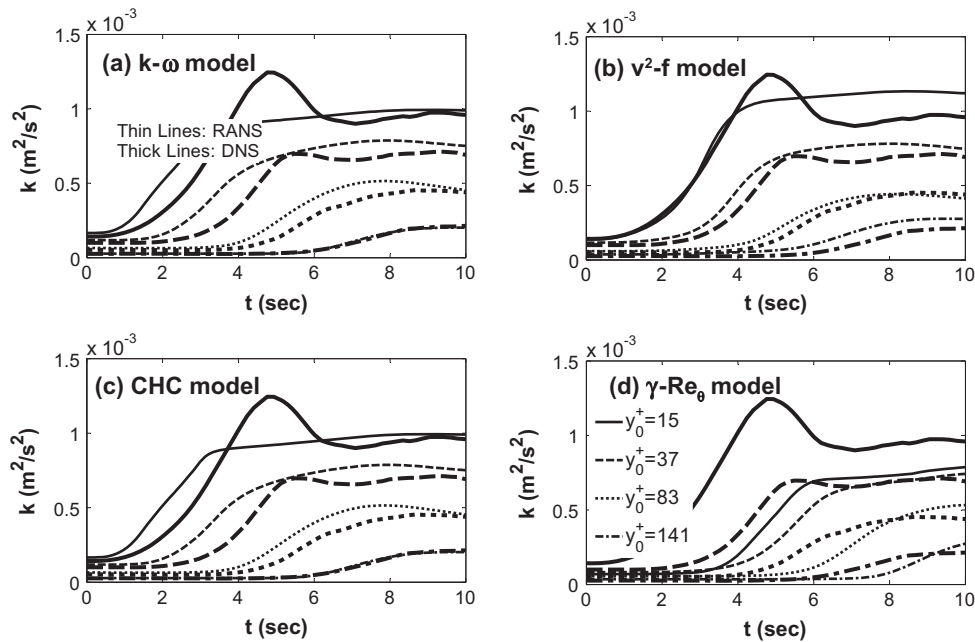

Fig. 11. Time-histories of turbulent kinetic energy at selected y_0^+ for unsteady flow case B: RANS model (thin lines) and DNS (thick lines).

kinetic energy so that both can be predicted faithfully. In principle, this is readily achievable with second momentum closure models. Regarding the performance of the models in the core region, all models reproduce the kinetic energy delay fairly well.

One of the main features of the turbulent viscosity formulation in the k–ε models considered in this study is the damping function (f_μ), the major role of which is to reduce turbulent viscosity in the wall region. Fig. 13 shows the across-channel profile of damping function f_μ at selected times, as predicted by four k–ε models (AB, YS, LB and CHC) for flow Case B. It is seen that the near-wall values of f_μ predicted by CHC is the only one that is sensitive to the imposed excursion. f_μ in CHC begins to respond to the imposed

flow rate immediately after the first stage of wall shear stress evolution (inertial-dominated period). The increased f_μ at the early stages of the excursion keeps turbulent kinetic energy and therefore turbulent shear stress low, reproducing the delay effect needed.

A damping function does not exist in the v^2–f or in the γ–Re_θ model. This correction function is replaced by the wall-normal stress component, as discussed in Section 2.3 for the v^2–f model. However, in the γ–Re_θ model the production of turbulent kinetic energy is controlled via intermittency factor derived from its transport equation. Fig. 14 shows the temporal evolution of the intermittency at selected y_0^+ for the three flow cases. It can be seen
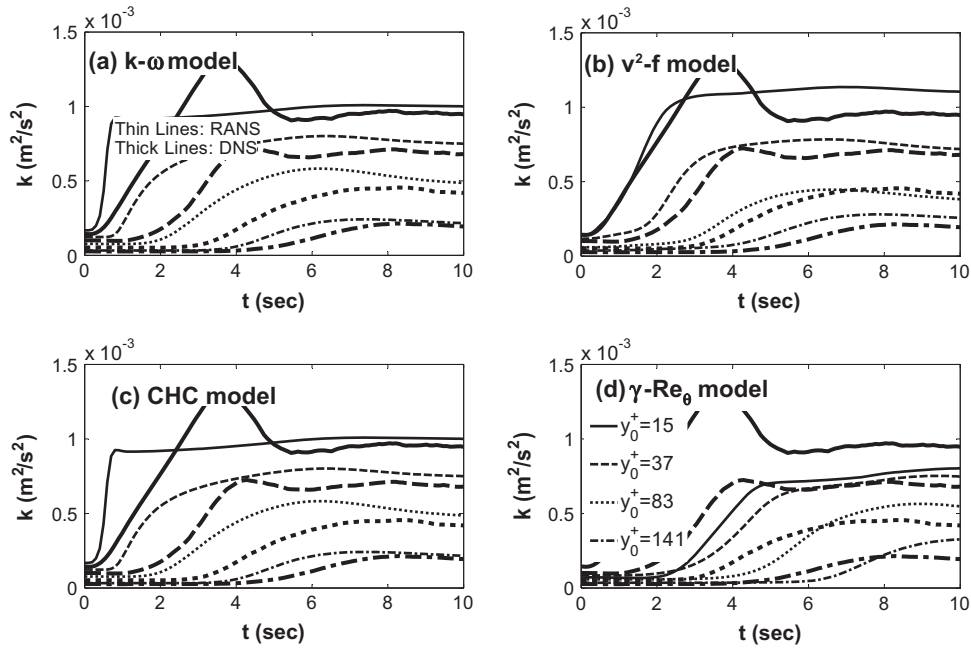
Fig. 12. Time-histories of turbulent kinetic energy at selected y_0^+ for unsteady flow case C: RANS model (thin lines) and DNS (thick lines).
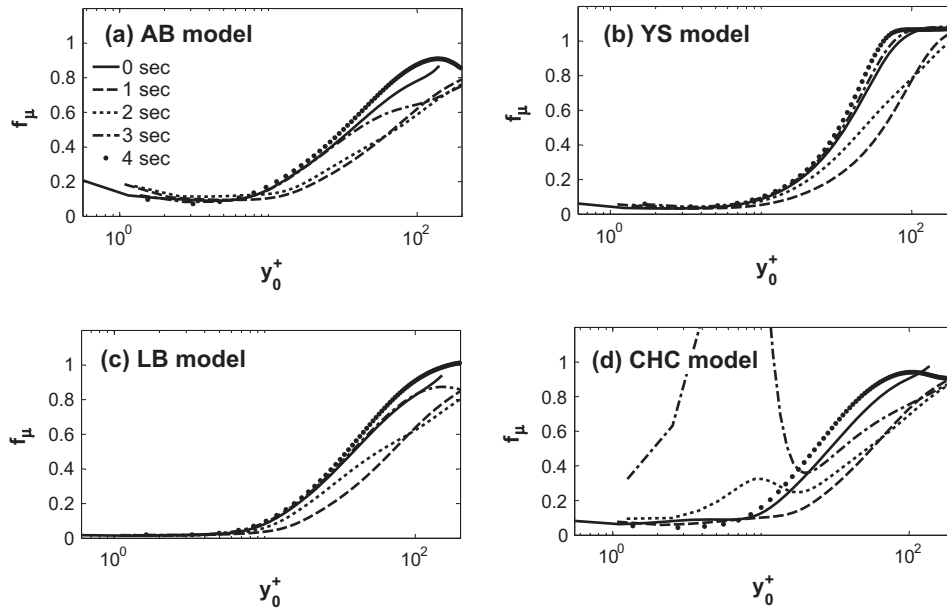

Fig. 13. Damping function profiles at selected times, as predicted by AB, YS, LB and CHC turbulence models for flow case B.

that the intermittency is reduced significantly at the early stages followed by a period of delay before increasing again. The turbulent viscosity trend shows similar behaviour. Such a reduction in the intermittency leads to further reduction in turbulent kinetic energy and shear stress in the wall region.

5. Conclusions

The performance of ten eddy viscosity turbulence models in predicting unsteady, ramp-up-type turbulent channel flows has been examined by comparing predictions with DNS results for the same flows. Three ramp-up flows with different acceleration rates have been considered. The key features of the unsteady flow as seen in the DNS data are the distinct delays in the response of the turbulent shear stress and turbulent viscosity to the imposed change in the flow rate. These delays are in turn responsible for the response of the wall shear stress. It is shown that the wall shear stress goes through a three-stage development. The first stage is influenced by the frozen turbulence and then inertia forces. In the early part of the first stage inertial forces dominate, causing the wall shear stress to overshoot the corresponding quasi-steady values. Then the effect of frozen (or delayed) turbulence takes over, causing the wall shear stress to undershoot the quasi-steady values. The second stage corresponds to rapid response of turbulence, causing rapid increase in wall shear stress. In the final stage the wall shear stress approaches the quasi-steady value.
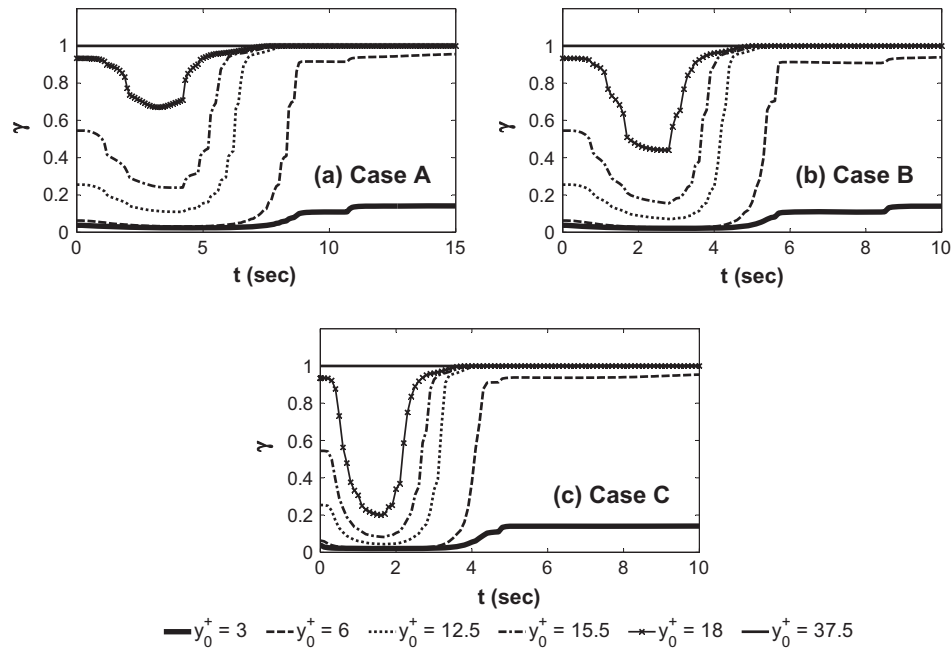
Fig. 14. Time-histories of intermittency at selected y_0^+, as predicted by γ–Re_θ for unsteady flow cases A, B and C.

Diffusion of turbulence from the wall to the core region is another feature of unsteady flows, leading to relatively long delays in the response of turbulent kinetic energy and turbulent shear stress in the core region. However, the duration of the delay period of turbulence response in the wall region is different for kinetic energy and for turbulent shear stress because of the stretching of turbulence structures.

The following are the main conclusions regarding the performance of the various turbulence models examined in this study:

• The most important feature that needs to be modelled in order to capture the overall behaviour of the flow is the delayed response of turbulent shear stress (and turbulent viscosity). Among the models examined, only the LS, CHC and γ–Re_θ models can capture this accurately, making them the only suitable models for such unsteady flows. LS and CHC achieve this through an appropriately designed damping function (f_μ), while γ–Re_θ employs an intermittency parameter that responds suitably to the variation in flow rate. However, it should be pointed out that the performance of the CHC model in high acceleration flow case was not satisfactory because of its instability. The AB and v^2–f model can also reproduce the basic trends but with much shorter time scales than expected.

• All models reproduce the overshoot in wall shear stress over the corresponding quasi-steady shear stress that occurs in the early stage of the flow rate excursion, with only minor differences between the predictions of each model. In fact, the overshoot is an inertia-dominated effect that is not related to turbulence. For this reason we expect the predictions of the various turbulence models to be similar at this early stage.

• The delay in the response of turbulence in the core region is governed by diffusion, represented explicitly in the transport equations of the k–ε/ω models. As a result, such delays are reasonably well predicted by all models.

• For accelerating flows, it is desirable that the early response of turbulent kinetic energy is not reflected in the model predictions unless turbulent kinetic energy and shear stress

formulations are decoupled. It is also noted that due to the similarities between channel and pipe flows, performance of turbulence models are expected to be similar for both geometries.

References

[1] Brereton GJ, Mankbadi RR. Review of recent advances in the study of unsteady turbulent internal flows. Appl Mech Rev 1995;48:189–212.
[2] Gündoğdu MY, Çarpinlioğlu MÖ. Present state of art on pulsatile flow theory (Part 2: Turbulent flow regime). JSME Int J Ser B: Fluids Thermal Eng 1999;42:398–410.
[3] Gerrard JH. An experimental investigation of pulsating turbulent water flow in a tube. J Fluid Mech 1971;46:43–64.
[4] Mizushina T, Maruyama T, Shiozaki Y. Pulsating turbulent flow in a tube. J Chem Eng Jpn 1973:6.
[5] Shemer L, Wygnanski I, Kit E. Pulsating flow in a pipe. J Fluid Mech 1985;153:313–37.
[6] Mao Z-X, Hanratty TJ. Studies of the wall shear stress in a turbulent pulsating pipe flow. J Fluid Mech 1986;170:545–64.
[7] Tardu SF, Binder G, Blackwelder RF. Turbulent channel flow with large-amplitude velocity oscillations. J Fluid Mech 1994;267:109–51.
[8] He S, Jackson JD. An experimental study of pulsating turbulent flow in a pipe. Eur J Mech B Fluids 2009;28:309–20.
[9] Scotti A, Piomelli U. Numerical simulation of pulsating turbulent channel flow. Phys Fluids 2001;13:1367–84.
[10] Scotti A, Piomelli U. Turbulence models in pulsating flows. AIAA J 2002;40:537–44.
[11] Cotton MA, Craft TJ, Guy AW, Launder BE. On modelling periodic motion with turbulence closures. Flow Turbul Combust 2001;67:143–58.
[12] Maruyama T, Kuribayashi T, Mizushina T. Structure of the turbulence in transient pipe flows. J Chem Eng Jpn 1976;9:431–9.
[13] Lefebvre PJ. Characterization of accelerating pipe flow. University of Rhode Island; 1987.
[14] He S, Jackson JD. A study of turbulence under conditions of transient flow in a pipe. J Fluid Mech 2000;408:1–38.
[15] Greenblatt D, Moss EA. Pipe-flow relaminarization by temporal acceleration. Phys Fluids 1999;11:3478–81.

[16] Greenblatt D, Moss EA. Rapid temporal acceleration of a turbulent pipe flow. J Fluid Mech 2004;514:65–75.
[17] He S, Ariyaratne C, Vardy AE. Wall shear stress in accelerating turbulent pipe flow. J Fluid Mech 2011;685:440–60.
[18] Chung YM. Unsteady turbulent flow with sudden pressure gradient changes. Int J Numer Meth Fluids 2005;47:925–30.
[19] He S, Ariyaratne C, Vardy AE. A computational study of wall friction and turbulence dynamics in accelerating pipe flows. Comput Fluids 2008;37:674–89.
[20] Ariyaratne C, He S, Vardy AE. Wall friction and turbulence dynamics in decelerating pipe flows. J Hydraul Res 2010;48:810–21.
[21] Seddighi M, He S, Orlandi P, Vardy AE. A comparative study of turbulence in ramp-up and ramp-down unsteady flows. Flow Turbul Combust 2011;86:439–54.
[22] Di Liberto M, Ciofalo M. Unsteady turbulence in plane channel flow. Comput Fluids 2011;49:258–75.
[23] Jung SY, Chung YM. Large-eddy simulation of accelerated turbulent flow in a circular pipe. Int J Heat Fluid Flow 2012;33:1–8.
[24] He S, Seddighi M. Turbulence in transient channel flow. J Fluid Mech 2013;715:60–102.
[25] He S, Ariyaratne C. Wall shear stress in the early stage of unsteady turbulent pipe flow. J Hydraulic Eng 2011;137:606–10.
[26] Patel VC, Rodi W, Scheuerer G. Turbulence models for near-wall and low Reynolds number flows. AIAA J 1985;23:1308–19.
[27] Myong HK, Kasagi N. New approach to the improvement of κ–ε turbulence model for wall-bounded shear flows. JSME Int J 1990;33:63–72.
[28] Chang KC, Hsieh WD, Chen CS. A modified low-Reynolds-number turbulence model applicable to recirculating flow in pipe expansion. J Fluids Eng Trans ASME 1995;117:417–23.
[29] Sarkar A, So RMC. A critical evaluation of near-wall two-equation models against direct numerical simulation data. Int J Heat Fluid Flow 1997;18:197–208.
[30] Launder BE. Low-Reynolds number turbulence near walls. Report TFD/86/4: UMIST; 1986.
[31] Tardu SF, Da Costa P. Experiments and modeling of an unsteady turbulent channel flow. AIAA J 2005;43:140–8.
[32] Al-Sharif SF, Cotton MA, Craft TJ. Reynolds stress transport models in unsteady and non-equilibrium turbulent flows. Int J Heat Fluid Flow 2010;31:401–8.
[33] Khaleghi A, Pasandideh-Fard M, Malek-Jafarian M, Chung YM. Assessment of common turbulence models under conditions of temporal acceleration in a pipe. J Appl Fluid Mech 2010;3:25–33.

[34] Revell AJ, Craft TJ, Laurence DR. Turbulence modelling of unsteady turbulent flows using the stress strain lag model. Flow Turbul Combust 2011;86:129–51.
[35] Shima N. Calculation of a variety of boundary layers with a second-moment closure applicable up to a wall. In: Proceedings of 7th symposium on turbulent shear flows. Stanford University; 1989. p. Paper 5–3.
[36] Launder BE, Sharma BI. Application of the energy-dissipation model of turbulence to the calculation of flow near a spinning disc. Lett Heat Mass Trans 1974;1:131–7.
[37] Durbin PA. Separated flow computations with the k–ε–υ^2 model. AIAA J 1995;33:659–64.
[38] Langtry RB, Menter FR. Correlation-based transition modeling for unstructured parallelized computational fluid dynamics codes. AIAA J 2009;47:2894–906.
[39] Abid R. Evaluation of two-equation turbulence models for predicting transitional flows. Int J Eng Sci 1993;31:831–40.
[40] Lam CKG, Bremhorst K. Modified form of the k-epsilon model for predicting wall turbulence. J Fluids Eng Trans ASME 1981;103:456–60.
[41] Yang Z, Shih TH. New time scale based k–ε model for near-wall turbulence. AIAA J 1993;31:1191–8.
[42] Abe K, Kondoh T, Nagano Y. A new turbulence model for predicting fluid flow and heat transfer in separating and reattaching flows-I. Flow field calculations. Int J Heat Mass Transf 1995;37:139–51.
[43] Mathur A, He S. Performance and implementation of the Launder–Sharma low-Reynolds number turbulence model. Comput Fluids 2013;79:134–9.
[44] Wilcox DC. Turbulence modeling for CFD. California: DCW Industries; 1998.
[45] Menter FR. Two-equation eddy-viscosity turbulence models for engineering applications. AIAA J 1994;32:1598–605.
[46] Durbin PA. Near-wall turbulence closure modeling without "damping functions". Theoret Comput Fluid Dyn 1991;3:1–13.
[47] Iaccarino G. Predictions of a turbulent separated flow using commercial CFD codes. Trans Am Soc Mech Eng J Fluids Eng 2001;123:819–28.
[48] Lien FS, Kalitzin G. Computations of transonic flow with the v^2–f turbulence model. Int J Heat Fluid Flow 2001;22:53–61.
[49] Abu-Ghannam BJ, Shaw R. Natural transition of boundary layers – the effects of turbulence, pressure gradient, and flow history. J Mech Eng Sci 1980;22:213–28.
[50] Mayle RE. The role of laminar-turbulent transition in gas turbine engines. J Turbomach 1991;113:509–37.
[51] Billard F, Laurence D. A robust k–ε–υ^2/k elliptic blending turbulence model applied to near-wall, separated and buoyant flows. Int J Heat Fluid Flow 2012;33:45–58.